PHYSICAL REVIEW B VOLUME 52, NUMBER 4 15 JULY 1995-II

Many-electron effects on ballistic transport

Yongjiang Wang
Centre for the Physics of Materials, Department of Physics, McGill University, Montréal, Québec, Canada H3A 2T8

Jian Wang
Department of Physics, The University of Hong Kong, Pokfulam Road, Hong Kong

Hong Guo
Centre for the Physics of Materials, Department of Physics, McGill University, Montréal, Québec, Canada H3A 2T8

Eugene Zaremba
Department of Physics, Queen's University, Kingston, Ontario, Canada K7L 3N6
(Received 15 August 1994; revised manuscript received 24 February 1995)

A Thomas-Fermi-Dirac–von Weizsäcker density-functional formalism is used to study the effects of many-electron Coulomb interactions on quantum transport through two-dimensional semiconductor nanostructures. The electron density is obtained by direct minimization of the total energy functional, and an effective potential for the electrons is determined as a functional of the density self-consistently. Transmission coefficient and conductance are computed with the effective potential included. The electron density distribution as well as the effective potential are strongly affected by the average electron density and the distance between the two-dimensional electron gas and the positive background charge. The transmission property of a stadium-shaped open quantum-dot system is investigated by varying these system parameters. The electron ballistic transport problem is solved in the presence of the many-electron effective potential and results are compared to that of the single-electron approximation. Some important differences are observed.

I. INTRODUCTION

In the past several years, considerable research efforts have been focused on the study of ultrasmall semiconductor structures, such as quantum wires and dots. With characteristic dimensions on the 100-nm scale, these systems have been fabricated from semiconductor heterostructures, which constrain the electrons to move in essentially a two-dimensional plane. The dimensionality of a two-dimensional (2D) electron gas can further be reduced to one or zero dimensions and a very rich variety of artificial solids are thus obtained.[1] This further reduction of dimensionality or confinement can now be routinely achieved by ionic etching or using metallic gates.[2] It is important to understand the electronic transport properties of these nanostructures with reduced dimensionality from both the fundamental physics point of view[3] and the prospects of device applications.[4] With a characteristic structure size comparable to the electron Fermi wavelength, the transport problems are usually treated as a quantum ballistic scattering process. In a theoretical investigation of ballistic transport, one computes transmission coefficients, which are related to conductance through Landauer formula[5] for two-probe systems, and through Büttiker formula[6] for multiprobe systems.

In most theoretical studies of quantum ballistic transport, some approximations are needed to simplify the calculation. For instance, one usually treats the confinement of the device structure using a hard wall potential. The single-electron and effective-mass approximations are also usually applied. Much progress has been made in these studies with qualitatively excellent and some times quantitatively good agreement with experimental measurements.[3] For instance, the experimental observation of Hall anomalies in quantum dots can be well explained by a ballistic resonant transport model;[7] the correlations in the magnetoconductance fluctuation of a classically chaotic billiard[8] maybe computed from single-electron scattering in such a structure;[9] the optics analogy of electron wave propagation through quantum wire systems can be investigated in detail[10–12] for its device applications.[13]

Given the success of our basic understanding of the ballistic quantum transport, it is desirable to move forward and examine some of the approximations in theoretical calculations. The purpose of this paper is to report our study of the effects of electron-electron Coulomb interactions to this transport regime.[14]

It is well known that many-electron interactions can change the effective confining potential profile of a device structure. Since the outcome of quantum scattering depends on the shape of the confining potential, the electronic transport properties of nanostructures will be affected by electron-electron interactions. For *closed* structures, the most used approach to include Coulomb interaction is the density-functional theory.[15] Using this method, Kumar *et al.* showed that the confining potential of a square-shaped quantum dot is actually circu-

larly symmetric and parabolic.[16] Further simplification using the Thomas-Fermi approximation has also been applied.[17] Recently, Zaremba and Tso[18] studied the collective excitations of a quantum-well structure using a Thomas-Fermi-Dirac–von Weizsäcker density-functional formalism; and Sun and Kirczenow studied the formation of quantum wires from electrostatic confinement.[19]

On the other hand, for *open* device structures with inhomogeneous electron systems, one deals with a scattering problem and it is difficult to include the Coulomb interactions. For a quasi-one-dimensional structure, the outgoing wave can be related to the incoming wave by a transfer matrix and this leads to some simplifications for studying the many-electron effects. One solves, for each incoming wave with momentum up to the Fermi level, the Schrödinger equation which includes the self-consistent potential as determined by the electron density. This is done for many incoming waves and the solutions of the Schrödinger equation are used to compute the electron density, which in turn determines the self-consistent potential. This process is iterated until self-consistency is achieved and the transmission coefficients are then obtained. Gawlinski and co-workers[20] applied this approach to the study of resonant tunneling diode, which is a one-dimensional structure. They concluded that in certain cases, the buildup of space charge inside the quantum well leads to changes of the confining potential and the peak-to-valley ratio of the tunneling current could be substantially altered by the electron-electron interactions.[20] While this approach is applicable in one-dimensional systems, it is very difficult to apply, if not impossible, to real two-dimensional structures. The main difficulty is due to the extremely large computational effort needed even for one dimension. Another problem is that there is no efficient two-dimensional transfer matrix to relate the outgoing wave to the incoming wave.

In the following, we shall present an approach to study the effects of electron-electron Coulomb interaction to ballistic transport in two-dimensional systems. The approach is based on a Thomas-Fermi-Dirac–von Weizsäcker[21] density-functional formalism. We first self-consistently solve the effective mean-field potential for the electrons for a given average electron density in a confined two-dimensional geometry. This is achieved by a direct minimization of the total energy functional.[22,23] With the effective potential, the transmission coefficients are then computed using a finite-element numerical scheme for solving the Schrödinger equation and transport properties are extracted. This approach allows us to include the direct Coulomb, electron ion, as well as the exchange-correlation interactions, and is completely general as for the device geometries. Compared with the one-dimensional method mentioned above, the savings of computational effort result for the following two reasons. First, instead of solving the Kohn-Sham equation, we have used the direct minimization scheme, which is much more efficient.[22] Second, we do not solve the transmission problem for each possible incoming wave separately, rather we compute the effective potential first and then study the transmission problem, which includes this effective potential. We have applied this approach to the study of transport through a stadium-shaped quantum dot structure connected to two external quantum wires. By comparing transmission coefficients with and without electron-electron interaction, we conclude that the interaction alters transport properties quantitatively and, furthermore, the exchange interaction plays a very substantial role.

The paper is organized as follows. In the next section, a sketch of 2D Thomas-Fermi-Dirac–von Weizsäcker density-functional formalism is given with a simple derivation of the von Weizsäcker term for completeness. In Sec. III, we use this formalism for the calculation of electron density and potential profile for a stadium-shaped quantum dot connected to two external quantum wires. In Sec. IV, the transmission coefficients is computed and results compared with those of the single-electron approximation. Finally, a short summary is presented in Sec. V.

II. THE DENSITY-FUNCTIONAL FORMALISM

The total energy of a many-electron system in standard density-functional theory is given by the following expression:

$$E[n] \equiv E[\{\psi_i\}] = \sum_i \int_\Omega d\mathbf{r}\psi_i^*(\mathbf{r})\left(-\frac{1}{2}\nabla^2\right)\psi_i(\mathbf{r}) + U[n], \quad (1)$$

where

$$U[n] = E_{\rm ee}[n] + E_{\rm exch}[n] + E_{\rm corr}[n] + E_{\rm ext}[n]\ . \quad (2)$$

Here, $n = n(\mathbf{r}) = \sum_i |\psi_i(\mathbf{r})|^2$ is the local electron density at position $\mathbf{r}$, computed from the occupied single-electron wave functions ψ_i. $U[n]$ is the potential energy expressed as a functional of the density $n(\mathbf{r})$ in the local density approximation. It includes the direct Coulomb energy $E_{\rm ee}$, the exchange energy $E_{\rm exch}$, the correlation energy $E_{\rm corr}$, and $E_{\rm ext}$ accounts for interaction with external fields, which includes the electron-ion interaction. Here, units are set such that $e = 1$ and $\hbar^2/m^* = 1$, where m^* is the electron effective mass. Using parameters for gallium arsenide, we have $m^* = 0.067m_0$, and dielectric constant $\epsilon = 13.18$. Therefore, the 2D electrons have an effective Bohr radius $a_B = \epsilon\hbar^2/m^*e^2 = 104.1$ Å and effective Rydberg $\mathcal{R}_y^* = m^*e^4/2\epsilon^2\hbar^2 = 5.25$ meV. The energy unit in the above equation is $2\mathcal{R}_y^* = 10.5$ meV.

The ground state energy is obtained by minimizing $E[n]$, with respect to the electron density n, and this leads to the well known Kohn-Sham equation.[15] Instead of solving the Kohn-Sham equation to minimize $E[n]$, we shall use an idea first proposed by Car and Parrinello,[22] which minimizes $E[n]$ by a direct method (see below). Furthermore, we notice that in $E[n]$ only the kinetic energy depends on the electron wave functions explicitly:

$$E_{\rm kin} = \sum_i \int_\Omega d\mathbf{r}\psi_i^*(\mathbf{r})\left(-\frac{1}{2}\nabla^2\right)\psi_i(\mathbf{r})\ , \quad (3)$$

thus, the computational effort in minimizing the energy functional will be drastically reduced if $E_{\rm kin}$ is also ex-

panded in terms of the local electron density $n(\mathbf{r})$. As mentioned above, for solid state structural and electronic calculations, such a gradient expanded kinetic-energy functional gives very good results compared with both full wave function calculations and experimental measurements.[18,23] In the following, a brief derivation of such an expanded kinetic-energy functional form is given for the 2D electron gas.

Following the procedure given in Ref. 24, the kinetic energy can be written in the form,

$$E_{\rm kin} = \int\int n(\mathbf{r}) f(k_F|\mathbf{r}-\mathbf{r}'|) n(\mathbf{r}') d\mathbf{r} d\mathbf{r}' \ , \tag{4}$$

where k_F is the Fermi momentum for the average electron density n_0 of the system. If we consider a noninteracting system with a density having only very small deviation from the homogeneous gas caused by a small potential perturbation $v(\mathbf{r})$, the total energy of system can thus be written as

$$E_{\rm tot} = \int\int n(\mathbf{r}) f(k_F|\mathbf{r}-\mathbf{r}'|) n(\mathbf{r}') d\mathbf{r} d\mathbf{r}' + \int v(\mathbf{r}) n(\mathbf{r}) d\mathbf{r} - E_f \int n(\mathbf{r}) d\mathbf{r} \ , \tag{5}$$

where $v(\mathbf{r})$ is the external field and E_f is the Lagrange multiplier to keep the total number of electrons fixed. Minimizing the energy functional, we get

$$2\int f(k_F|\mathbf{r}-\mathbf{r}'|) n(\mathbf{r}') d\mathbf{r}' + v(\mathbf{r}') - E_f = 0 \ . \tag{6}$$

Assuming the perturbation form from the uniform density, i.e., $n(\mathbf{r}) = n_0 + \Delta n(\mathbf{r})$, we have the following two equations:

$$2n_0 \int f(k_F|\mathbf{r}-\mathbf{r}'|) d\mathbf{r}' - E_f = 0 \ , \tag{7}$$

$$2\int f(k_F|\mathbf{r}-\mathbf{r}'|) \Delta n(\mathbf{r}') d^3\mathbf{r}' + v(\mathbf{r}') = 0 \ , \tag{8}$$

or in k space,

$$2F(k)\Delta N(k) = -V(k) \ , \tag{9}$$

where $F(k)$, $\Delta N(k)$, and $\Delta V(k)$ are Fourier transforms of f, Δn, and v, respectively. Comparing with the linear response theory,[25] we have

$$F(k) = \frac{1}{2G(k)}, \tag{10}$$

where $G(k)$ is the Green's function[25] and for large k,

$$G(k) = \frac{1}{\pi}[1 - \sqrt{1-(2k_F/k)^2}] \sim \frac{1}{\pi}\left[\frac{2k_F^2}{k^2} + \frac{2k_F^4}{k^4} + \frac{4k_F^6}{k^6}\right] \ . \tag{11}$$

On the other hand when k is zero, from Ref. 25, $G^{-1}(0) = \pi$. Now we introduce the function $w(k)$,

$$w(k) \equiv G^{-1}(k) - \frac{\pi}{2}\frac{k^2}{k_F^2} + \frac{\pi}{2} \ . \tag{12}$$

Thus, $F(k)$ is rewritten as

$$F(k) = \frac{1}{2G(k)} = \frac{1}{2}w(k) + \frac{\pi}{4}\frac{k^2}{k_F^2} - \frac{\pi}{4} \ . \tag{13}$$

Using the above expression, the kinetic energy can be written as

$$E_{\rm kin} = \frac{1}{2}\int\int n(\mathbf{r}) w(|\mathbf{r}-\mathbf{r}'|) n(\mathbf{r}') d\mathbf{r} d\mathbf{r}' - \frac{\pi}{4}\int n^2(\mathbf{r}) d\mathbf{r} + \frac{\pi}{4}\int |n(k)|^2 \frac{k^2}{k_F^2} dk \ . \tag{14}$$

Since for 2D homogeneous electron gas $n_0 = k_F^2/(2\pi)$, we have

$$\frac{\pi}{4}\int |n(k)|^2 \frac{k^2}{k_F^2} dk = \frac{1}{8n_0}\int |\nabla n(\mathbf{r})|^2 d^3\mathbf{r} \approx \frac{1}{8}\int \frac{|\nabla n(\mathbf{r})|^2}{n(\mathbf{r})} d^3\mathbf{r} \ , \tag{15}$$

where the last approximation is valid up to quadratic order. Finally, we arrive at

$$E_{\rm kin} = \frac{1}{2}\int\int n(\mathbf{r}) w(|\mathbf{r}-\mathbf{r}'|) n(\mathbf{r}') d^3\mathbf{r} d^3\mathbf{r}' - \frac{\pi}{4}\int n^2(\mathbf{r}) d^3\mathbf{r} + \frac{1}{8}\int \frac{|\nabla n(\mathbf{r})|^2}{n(\mathbf{r})} d^3\mathbf{r} \ , \tag{16}$$

where $w(k)$ is given by Eq. (12). When the variation of the density is slow, one has

$$\int n(\mathbf{r}') w(|\mathbf{r}-\mathbf{r}'|) d^3\mathbf{r}' \approx n(\mathbf{r}) \int w(|\mathbf{r}-\mathbf{r}'|) d^3\mathbf{r}' = n(\mathbf{r}) W(k=0) = \frac{3\pi}{2} n(\mathbf{r}). \tag{17}$$

So the first two terms of Eq. (16) give the Thomas-Fermi term for 2D electron gas and the last term is the corresponding von Weizsäcker correction; finally, we have

$$E_{\rm kin} = \int d\mathbf{r}\left[\frac{\pi}{2} n^2(\mathbf{r}) + \lambda \frac{|\nabla n(\mathbf{r})|^2}{n(\mathbf{r})}\right], \tag{18}$$

where $\lambda = 1/8$.

The first term in the potential energy (2) is the direct Coulomb interaction energy,

$$E_{\rm ee} = \frac{1}{2}\int d\mathbf{r}\int d\mathbf{r}_1 \frac{n(\mathbf{r}) n(\mathbf{r}_1)}{|\mathbf{r}-\mathbf{r}_1|} \ .$$

For 2D electron gas, the exchange and correlation energies can be written as[26]

$$E_{\rm exch} = -\lambda_x n^{3/2}(\mathbf{r}) \ ,$$

$$E_{\rm corr} = -0.9775 \int d\mathbf{r} \frac{n^{3/2}(\mathbf{r})}{1 + 7.8165 n^{1/2}(\mathbf{r})} \ ,$$

where $\lambda_x = 1.0638$. The last term $E_{\rm ext}$ of (2) accounts for contributions from external potentials. In our case, it includes the potential from the positive charge background, whose charge density is such that the total net charge is zero; it also includes the external confining potential, which could be provided by metallic gating for the device geometry.

Although it is straightforward to include all the terms listed above for the total energy functional, in the following we shall neglect the correlation energy, because it is numerically small compared with other terms. Collecting all terms, the total energy is written as

$$E[n] = \int d\mathbf{r}\left[\frac{\pi}{2}n^2(\mathbf{r}) + \lambda\frac{|\nabla n(\mathbf{r})|^2}{n(\mathbf{r})} - \lambda_x n^{3/2}(\mathbf{r})\right] + \frac{1}{2}\int d\mathbf{r}\int d\mathbf{r_1}\frac{n(\mathbf{r})n(\mathbf{r_1})}{|\mathbf{r}-\mathbf{r_1}|} + \int d\mathbf{r} n(\mathbf{r})v_{\rm ext}(\mathbf{r}) \ , \tag{19}$$

where the last term gives $E_{\rm ext}$.

To obtain the electron density distribution of the ground state the total energy functional $E[n]$ is minimized, with respect to n under the constraint that the number of electrons is kept constant, i.e.,

$$\int d\mathbf{r} n(\mathbf{r}) \ = \ N \ . \tag{20}$$

Since n is non-negative, it is often convenient to use χ with $n \equiv \chi^2$ as the variable. Requiring

$$\delta E[\chi]/\delta\chi(\mathbf{r}) = 0 \tag{21}$$

and from Eq. (19), we have

$$2\pi\chi^3 - \nabla^2\chi + 2\chi\int d\mathbf{r}'\frac{\chi^2(\mathbf{r}')}{|\mathbf{r}-\mathbf{r}'|} - 3\lambda_x\chi^2 + v_{\rm ext}(\mathbf{r}) = 0 \ , \tag{22}$$

which must be solved under the constraint (20).

For complicated two-dimensional device structures, solving the nonlinear partial differential equation (22) is difficult and inefficient. As mentioned in the Introduction, instead of solving this equation, we directly minimized $E[n]$ using a simple steepest descent method by iterating the local function $\chi(\mathbf{r})$ until the total energy is minimized. This is achieved by the following equation subjecting to the constraint (20):

$$\chi^{(m+1)} \ = \ \chi^{(m)} \ - \Delta\frac{\delta E[\chi]}{\delta\chi(\mathbf{r})} \ , \tag{23}$$

where the function $\chi(\mathbf{r})$ of the $(m+1)$th iteration is obtained from its values at the mth iteration. Here, Δ is a "time" step for the iteration which was chosen small enough to maintain the stability of the iteration procedure, but large enough for fast convergence. One can easily see that at convergence, i.e., $\chi^{m+1}(\mathbf{r}) = \chi^m(\mathbf{r})$, Eq. (23) reduces to Eq. (21), thus this procedure is equivalent to solving Eq. (22). Finally, after the electron density $n(\mathbf{r})$, which minimizes $E[n]$, is obtained, the effective potential for the electrons can be computed,

$$V_{\rm eff}(\mathbf{r}) = \frac{\partial}{\partial n(\mathbf{r})}(E_{\rm ee}[n] + E_{\rm exch}[n] + E_{\rm ext}[n]) \ . \tag{24}$$

$V_{\rm eff}$ will then be used to compute the transmission coefficients and other transport properties of a device structure. In the next section, this formalism is applied to study ballistic transport through a stadium-shaped quantum-dot system. Boundary conditions for iterating (23) will also be discussed.

III. DENSITY AND EFFECTIVE POTENTIAL OF A QUANTUM DOT

We now apply the approach outlined in the previous section to calculate the effective potential of an open stadium-shaped quantum dot. Recently, this structure has attracted much attention[8,9] because it provides a testing ground for the studies of quantum chaos via ballistic electron transport properties. The schematic view of the structure is shown in Fig. 1, in which the quantum wires and the stadium-shaped dot are divided into five regions labeled I–V.

When quantum wires are connected to a device structure, they form an open system where electrons are allowed to flow in and out of the device. Here, we assumed that the quantum wires extend far to the left of region I and to the right of region V. We need to fix the boundary conditions at the left end of region I and the right end of region V, i.e., at the open ends of the leads to the quantum dot. Note that in the quantum wires very far away from the scattering region, the electron density distribution should be close to that in an infinitely long uniform quantum wire. Thus, we may fix one of the boundary conditions by $n(x_0, y) = n_{\rm inf}(y)$, where $\mathbf{r_0} \equiv (x_0, y)$ is the coordinates of the open ends, and $n_{\rm inf}(y)$ is the charge density in an infinitely long quantum wire with the same average density n_0. Obviously, $n_{\rm inf}$ is only a function of the y coordinate. As another boundary condition, we required that the charge densities match smoothly at the open ends, $\nabla n(\mathbf{r})|_{\mathbf{r}=\mathbf{r_0}} \cdot \hat{x} = 0$, where $\hat{x}$ is the unit vector along the x direction.[27] With these boundary conditions, the procedure outline in the last section can be carried out.

To be specific, we have chosen the width of the quantum wire $a = 10a_B = 1041$ Å, the radius of the circular part of the stadium is $a/2$, and the length of the rectangle part along y direction is $7a/5$. To implement the algorithm numerically, the regions I–V were discretized with 5480 uniformly distributed grid points. The dis-

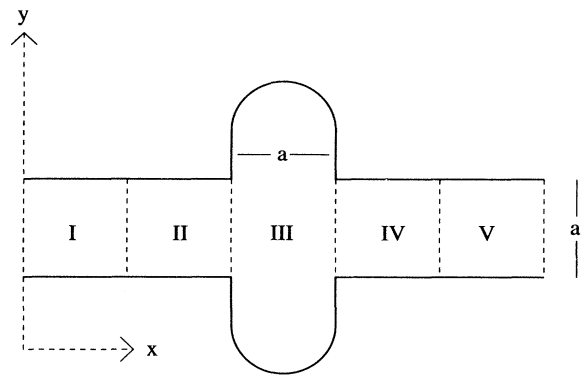

FIG. 1. Schematic view of the stadium-shaped quantum wire structure. Here, the width of the wire is $a = 10a_B$ and the radius of the circular part of the stadium shape is $r = 5a_B$, with a_B the effective Bohr radius, $a_B = 104.1$ Å. The rectangular part of the stadium shape has a length $14a_B$.

tances from the two open ends of the quantum wires to the dot region are both $2a$, while the width of the stadium is a. At this distance, it is a good approximation to apply the boundary condition to the two open ends of the discretization region, as will be shown by the results obtained in the following. The density distribution at the two open ends was obtained by solving the density-functional problem for a uniform quantum wire.

Figures 2(a) and 2(b) show the lateral density and potential profile across a uniform quantum wire with an average electron density $n_0 = 0.5/a_B^2$ in unit of the effective Bohr radius $a_B = 104.1$ Å. The distance between the 2D electron gas and the positive background charge, i.e., the electrons-ions distance is taken as $z = 3a_B$. Hard wall boundary conditions are assumed at the walls for the quantum wire, which provides confinement for the electrons. The general feature of quantum wire density and potential are quite similar to results of a Kohn-Sham density-functional approach obtained by Sun and Kirczenow,[19] where they considered the case of electron confinement by pure Coulomb attraction from the positive ion charges. The effective potential is determined by the combined profile of direct Coulomb potential, exchange potential, as well as the hard wall confining potential as one can see from Eq. (24). Also shown in Fig. 2(b) are effective potential contributions from direct Coulomb interaction, and the exchange potential due to the Dirac-exchange term in Eq. (19). We can see that the exchange term gives rise to a negative potential, while the direct Coulomb interaction is positive and leads to a overall positive potential for the quantum wire. For this uniform quantum wire, we notice that the Dirac-exchange energy results in a very flat negative potential, indicating that a Hartree calculation should be a good approximation in this case. It is clear that the direct Coulomb and exchange interactions are strongly affected by the distance z between the electron gas and the positive ion dopant charges, and also by the average linear electron density n_l in the quantum wire. With the decrease of z screening effects get stronger, leading to a reduction of direct Coulomb energy and a growing relative contribution of the exchange energy, which could even give an overall negative effective potential inside the wire.

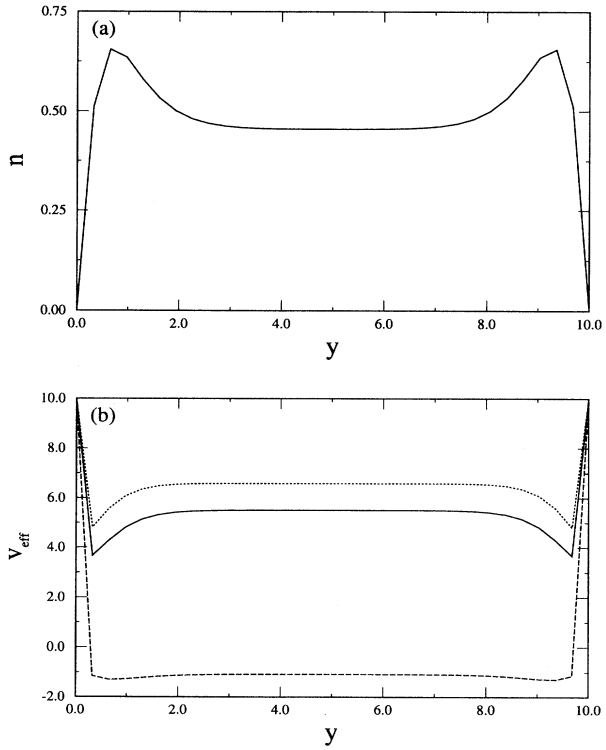

FIG. 2. Density and potential profiles along the y direction in the quantum wire. Length in unit of a_B, potential in the unit of $2R_y = 10.5$ meV. (a) The electron density. Parameters used: average density $n_0 = 0.5/a_B^2$; distance between electrons and the positive charge background $z = 3a_B$. (b) The effective potential profile (solid line) corresponding to the density in (a). The dotted line is the effective potential resulting from only the direct Coulomb interaction. The dashed line is the exchange potential.

With the effective potential obtained, the electron subband energy of the quantum wire can be computed. In the unit of $2\mathcal{R}_y^*$ the first and the second subband energies are 5.492 and 5.549, respectively. The Fermi energy of the quantum wire is determined by

$$\sum_{E_i \le E_f} \frac{2}{\pi} \left[\frac{2m^*(E_f - E_i)}{\hbar^2} \right]^{1/2} = n_l \ , \tag{25}$$

where E_f is the Fermi energy, E_i is the ith subband threshold energy, and n_l is the linear density of the quantum wire. We obtained $E_f = 5.494$. The fact that the Fermi energy is very close to the first subband threshold energy is an indication of strong confinement due to the hard wall condition. This is also true for smaller electron densities. For $n_0 = 0.1/a_B^2$, corresponding to a linear density of $n_l = 1.0/a_B$, the first and second subband energies are 0.985 and 1.076 respectively, while the Fermi energy is $E_f = 0.989$, still very close to the first subband.

Having computed the density profile of a uniform quantum wire thus fixing the boundary conditions as discussed above, we can now iterate Eq. (23) for the energy functional minimization of the entire structure including the quantum dot. Typically convergence was obtained with about 2000 iteration steps. Figure 3 is a plot of the density distribution in region II, III, IV, with $n_0 = 0.5/a_B^2$ and $z = 3a_B$. The density profile in the leads becomes uniform along the x direction very rapidly away from the region III, indicating that the open boundary conditions specified above are extremely well satisfied. Also, we notice that the density variation is generally smooth and small, except near the hard wall boundary, where density drops to zero. This suggests that the Thomas-Fermi-Dirac–von Weizsäcker formalism, which is based on the assumption of small density variations, is an appropriate approach for quantum wire structures even with sharp geometry distortion like the one considered here.

Figure 4(a) shows the effective potential profile along the line bisecting the quantum dot and perpendicular to the wires, with and without the exchange term. It is

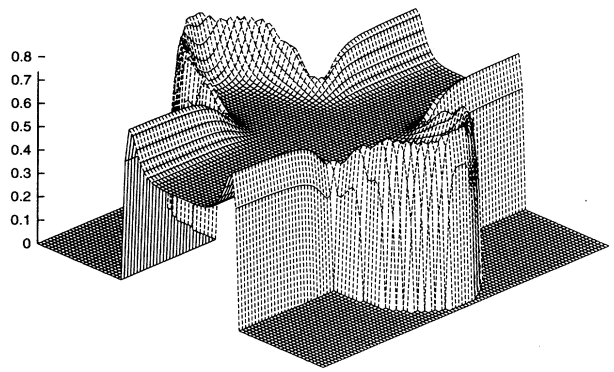

FIG. 3. Three-dimensional plot of the electron density profile (the vertical axis) for regions II, III, IV of Fig. 1. The average density n_0 and electron-ion distance z are the same as in Fig. 2(a).

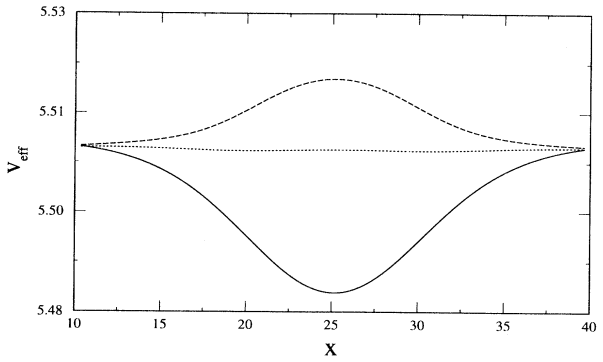

FIG. 5. Potential profiles for different electron-ion distances $z = 3a_B$ (solid line), $z = a_B$ (dotted line), and $z = 0$ (dashed line). The average electron density is fixed at $n_0 = 0.5/a_B^2$. The units are the same as in Fig. 2(a).

quite similar to that for uniform quantum wire, Fig. 2. The potential inside the quantum dot is very smooth and varying only slightly, except near the hard wall boundary, where a narrow potential valley is created. This valley has the effect of attracting electron to its positions, a reflection of Coulomb repulsion. Figure 4(b) shows the

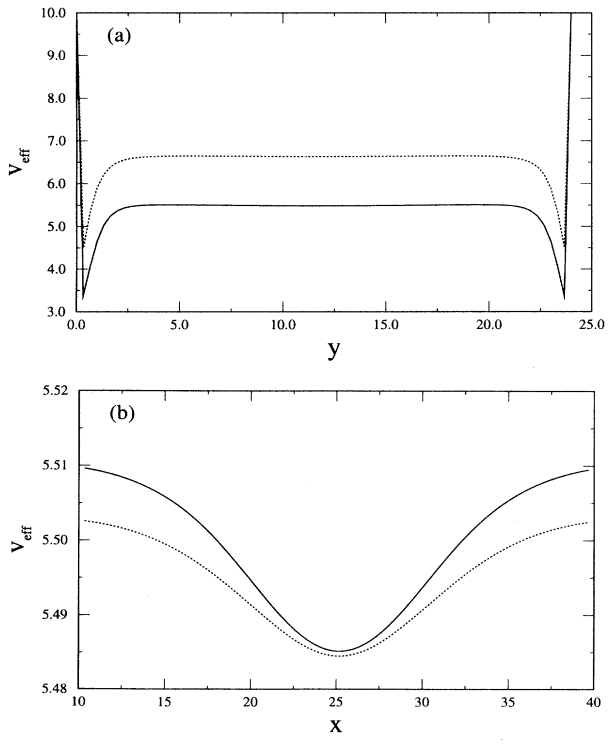

FIG. 4. Lateral potential profiles with (solid line) and without (dotted line) the exchange interaction. The parameters n_0 and z and units of axis are the same as in Fig. 2. (a) Along the y direction bisecting the stadium-shaped dot. (b) Along the x direction across regions II, III, IV on the center line of the quantum wire.

effective potential across the quantum-dot region along the bisecting line of the quantum wire. The electron density inside the dot region is greater than that outside and correspondingly there is a potential well inside the dot, as shown in Fig. 4(b). This will affect the electron transport behavior, as we will discuss later. We found that the exchange interaction does not seem to substantially change the density distribution, but it contributes substantially to the total energy. Another effect of the exchange is that it makes the potential well along x-direction steeper [Fig. 4(b)], thus affecting the transmission behavior.[28]

It is of practical interest to see how the changes in distance between the background ion charges and the electron gas will affect the results. We have calculated three different cases with this distances to be $z = 3a_B$, $z = a_B$, and the limiting case of $z = 0$, respectively, keeping average electron density $n_0 = 0.5/a_B^2$. As mentioned above, this has considerable effects on the density and potential profiles in the dot. For larger z the screening effect is reduced, thus, the direct Coulomb interaction pushes electrons outward building a larger density near the wall boundaries. This leads to a deeper and steeper potential valley near the wall boundary. Along the bisecting line of the quantum dot in the x direction, Fig. 5 shows the potential profile with z decreasing from $z = 3a_B$ to $z = 0$. We found that the potential well structure inside the dot changes to a potential barrier when the distance is decreased.[29] The general trend is that with the increase of z the positive direct Coulomb potential increases rather quickly, while the exchange is almost unaffected. We conclude that the combined effects of confinement from the walls of the quantum dot and the electron-electron, electron-ion interactions can make rather different shapes of the effective potential along the quantum wires crossing through the quantum dot. This can cause important differences in transmission through the structure.

IV. EFFECTS TO THE BALLISTIC TRANSPORT

In many cases the electron transport in nanostructures at low temperature have been treated as a quantum bal-

listic transmission problem, i.e., free of impurity scattering and electron-phonon interactions. Therefore, the ballistic transport problem is solely determined by the scattering of electron from the confining potential of a specific structure. In the single-electron approximation, the confining potential is provided by the geometry boundary of a nanostructure. With Coulomb interactions evaluated within a mean-field picture, we may study ballistic transport of an electron through the effective potential as described in the last section. Since the effective potential is a combined result from external confinement, the electron-electron and the electron-ion interactions, this is a first approximation within the mean-field approach to investigate the Coulomb effects to ballistic transport.

In order to solve the Shrödinger equation for the scattering problem including a complicated potential, we use a finite-element numerical scheme,[30,31] which divides the structure into probe regions and the scattering region (quantum dot). The wave function inside the scattering region is expressed using finite-element expansion, while the probe region can be solved numerically as a 1D problem. Matching of the wave functions and their normal derivatives at the regional boundaries leads to linear algebraic equations, which are solved to give transmission coefficients as well as other quantities of interests. Usually about 3000 nodal points have been used in the quantum-dot region for the finite-element discretization. For details of this scheme, see Refs. 30, 31.

Figure 6 shows the transmission coefficients versus incident electron energy with and without the Coulomb effects. We only calculated transmission coefficients within the range of the first transport subband. The effective potential is obtained for the average density $n_0 = 0.5/a_B^2$ and electron-ion distance $z = 3a_B$. To compare the transmission coefficients of the two cases (with or without the electron-electron interaction), we have shifted all the quantum wire eigenvalues (the subband threshold energies) for the many-electron case by a constant factor, so

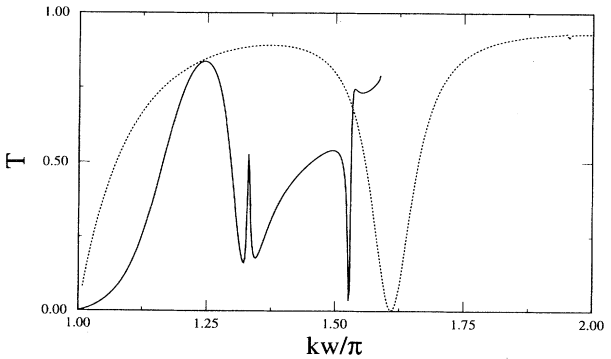

FIG. 6. Transmission coefficient including the Coulomb effects (solid line) and the corresponding result of the single-electron approximation (dotted line). The transmission coefficients are plotted against kW/π, where k is determined by the incident electron energy E, $E = \hbar^2k^2/2m^*$. $W = 10a_B$ is the width of the quantum wire. The effective potential is obtained for parameters $z = 3a_B$ and $n_0 = 0.5/a_B^2$.

that the first subband threshold energy aligns with that of the single-electron value $E_1 = \hbar^2\pi^2/2m^*W^2$. This constant shift does not affect the physics. Figure 6 shows that the energy range for electron transporting purely in the first subband is smaller when Coulomb effects are included. For the single-electron approximation, the first subband is from $kW/\pi = 1$ to $kW/\pi = 2$, while it is from $kW/\pi = 1$ to $kW/\pi = 1.6$ in the many-electron case. The fact that the energy range of the first subband transport can be changed significantly is a consequence of the more general result that the eigenenergy spacing of the quantum structure is changed after including the Coulomb effects. Also, as we have seen in the last section, the effective potential is always smoother than the hard wall confinement alone, thus, the sharp constrictions and corners often seen in model calculations of ballistic transport will be rounded off by Coulomb effects. These may have important implications for understanding of many transport phenomena. For example, in the study of quantum chaotic motion of electrons in a ballistic structure,[32,9,8] one uses the nature of the statistics of quantum level spacings to classify the motion as regular or chaotic.[33] Since electron-electron Coulomb interaction changes the single particle levels, it may alter the level statistics, such that a nonchaotic billiard for a single electron may become chaotic, as the effective potential due to many electrons can be quite different from the billiard shape.

Besides the energy range change, there are more fluctuations in the transmission coefficient (thus also in the conductance) for the case with Coulomb effects, compared with the generally smooth pattern of the single-electron transport. The fluctuation is a result of quantum interference and is determined by the scattering of electron wave from the effective confining potential of a particular structure. The greater fluctuation is an indication of the effective potential variation for the many-electron case, as opposed to the simple hard wall single-electron confinement. Also in many circumstances, the transmission variations are related to the existence of quasibound states (resonant states), this is especially true in cases with sharp conductance peaks or dips.[34] The more rapid fluctuation thus may also suggest a richer quasibound state spectrum when a many-electron effective potential is included.

The solid line in Fig. 7(a) is the transmission curve for a lower average electron density of $n_0 = 0.1/a_B^2$ or equivalently $1.0 \times 10^{11}/\text{cm}^2$. We find that it is smoother and with a larger energy gap between first and second subband thresholds, compared with the higher density case of $n_0 = 0.5/a_B^2$ (dotted line). With reduced electron density, the Coulomb effects are reduced and the conductance of the structure should be closer to that of the single-electron approximation, as observed here. As discussed in the last section, a reduction of the electron-ion distance also reduces the electron-electron Coulomb interaction, due to stronger screening. This should have the same effect as reducing n_0. In Fig. 7(b), we compare the transmission coefficients for the same n_0, but with different z. Indeed for the case with smaller distance (solid line), $z = a_B$, the transmission curve is smoother

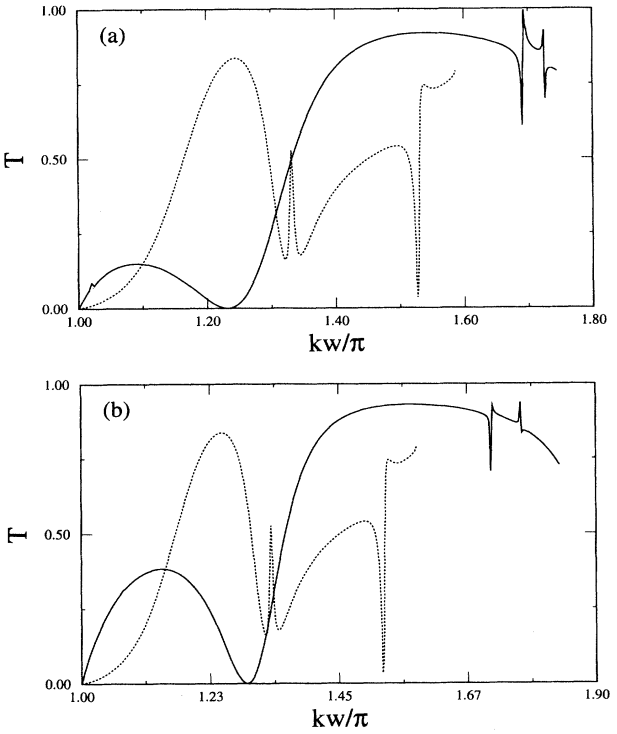

FIG. 7. (a) A comparison of transmission obtained using effective potentials for $n_0 = 0.1/a_B^2$ (solid line) and for $n_0 = 0.5/a_B^2$ (dotted line) with $z = 3a_B$. (b) A comparison of transmission obtained using effective potentials for two different electron-ion distances $z = a_B$ (solid line) and $z = 3a_B$ (dotted line), with the average density $n_0 = 0.5/a_B^2$.

and the energy interval between the first and second subband threshold energy is larger, in comparison with the case of $z = 3.0a_B$ (dotted line).

V. SUMMARY

We have studied the effects of many-electron Coulomb interaction to the effective potential profile of an *open* two-dimensional quantum dot structure, using a Thomas-Fermi-Dirac–von Weizsäcker density-functional formalism. A direct minimization of the total energy is very efficient in obtaining the ground state energy and the electron density profile. The method used here is completely general and is not restricted to two probe quantum structures. An external magnetic field can also be included at least at the Hartree level. The computational effort is moderate.[35]

Apart from the direct Coulomb interaction energy, we found that the exchange interaction contributes significantly to the effective potential. The average electron density, as well as the distance between electrons and positive charge background have substantial influences on the effective potential. As the average density is increased, the direct Coulomb interaction energy increases rapidly, while the exchange interaction changes relatively slowly and is more significant in the case of lower density. The effects of the many-electron interaction on the ballistic electron transport is studied by including the effective potential obtained from the density-functional approach into the scattering problem. The single-electron scattering by the effective potential inside the stadium-shaped quantum dot is solved using a finite element numerical approach. The transmission coefficient thus obtained is compared to the corresponding result without the many-electron effects. It is found that the energy interval between the first and second subband energy threshold has changed significantly. Also, the fluctuation in the transmission coefficients is quite different with or without the many-electron potential. However, when the density of the electron gas or the distance between electron gas and the positive charge background is reduced, many electron effects on the ballistic transport are reduced. In this case, the feature of conductance variation is more close to the results of a single-electron approximation.

ACKNOWLEDGMENTS

This work was supported by the Natural Sciences and Engineering Research Council of Canada and le Fonds pour la Formation de Chercheurs et l'Aide à la Recherche de la Province du Québec.

[1]Marc A. Kastner, Phys. Today **46** (1), 24 (1993).
[2]M. Roukes, T. Thornton, A. Scherer, J. Simmons, B. Van der Gaag, and E. Beebe, in *Science and Engineering of 1- and 0-Dimensional Semiconductors*, edited by S. Beaumont and C. Sotomayer-Torres (Plenum, London, 1990).
[3]C. W. J. Beenakker and H. Van Houten, in *Solid State Physics, Advances in Research and Applications*, edited by H. Ehrenreich and D. Turnbull (Academic, San Diego, 1991), Vol. 44.
[4]See, for example, *Physics of Quantum Electron Devices*, edited by F. Cappaso, Springer Series in Electronics and Photonics Vol. 28 (Springer, Berlin, 1990).
[5]R. Landauer, IBM J. Res. Dev. **1**, 233 (1957); Philos. Mag. **21**, 863 (1970).
[6]M. Büttiker, IBM J. Res. Dev. **32**, 317 (1988).
[7]G. Kirczenow and E. Castaño, Phys. Rev. B **43**, 7343 (1991); C. J. B. Ford, S. Washburn, R. Newbury, C. M. Knoedler, and J. M. Hong, *ibid.* **43**, 7334 (1991).
[8]C. M. Marcus, A. J. Rimberg, R. M. Westervelt, P. F. Hopkins, and A. C. Gossard, Phys. Rev. Lett. **69**, 506 (1992).
[9]Y. Wang, J. Wang, H. Guo, and C. Roland, J. Phys. C **6** L143 (1994); H. Baranger, R. Jalabert, and A. Stone, Phys. Rev. Lett. **70**, 3876 (1993).
[10]J. Wang, H. Guo, and R. Harris, Appl. Phys. Lett. **57**, 3075 (1991); J. Wang, Y. J. Wang, and H. Guo, Phys. Rev. B **46**, 2420 (1992).
[11]S. Datta (unpublished).
[12]F. Sols, M. Macucci, U. Ravaioli, and K. Hess, Appl. Phys.

Lett. **54**, 350 (1989).
[13]J. A. del Alamo and C. C. Eugster, Appl. Phys. Lett. **56**, 78 (1990); N. Tsukada, A. D. Wieck, and K. Ploog, *ibid.* **56**, 2527 (1990).
[14]As a short account see, J. Wang, Y. Wang, and H. Guo, J. Appl. Phys. **75**, 2721 (1994).
[15]W. Kohn and L. J. Sham, Phys. Rev. **140**, A1133 (1965); G. P. Srivastava and D. Weaire, Adv. Phys. **36**, 463 (1987).
[16]See, for example, A. Kumar, S. E. Laux, and F. Stern, Phys. Rev. B **42**, 5166 (1990); W. Lai and S. Das Sarma, *ibid.* **33**, 8874 (1986); S. Laux and F. Stern, Appl. Phys. Lett. **49**, 91 (1986).
[17]J. Nixon and J. Davies, Phys. Rev. B **41**, 7929 (1990); J. Luscombe and M. Luban, Appl. Phys. Lett. **57**, 61 (1990); L. Glazman and I. Larkin, Superlatt. Microstruct. **6**, 32 (1991).
[18]E. Zaremba and H. Tso, Phys. Rev. B **49**, 8147 (1994).
[19]Y. Sun and G. Kirczenow, Phys. Rev. B **47**, 4413 (1993).
[20]E. Gawlinski, T. Dzurak, and R. Tahir-Kheli, J. Appl. Phys. **72**, 3562 (1992).
[21]C. F. von Weizsäcker, Z. Phys. **96**, 431 (1935).
[22]R. Car and M. Parrinello, Phys. Rev. Lett. **55**, 2471 (1985).
[23]N. Govind, J. Wang, and H. Guo, Phys. Rev. B **50**, 11 175 (1994).
[24]L. W. Wang and M. P. Teter, Phys. Rev. B **45**, 13 196 (1992).
[25]T. Ando, A. Fowler, and F. Stern, Rev. Mod. Phys. **54**, 437 (1982).
[26]M. Jonson, J. Phys. C **9**, 3055 (1976).
[27]While the set of boundary conditions used here are quite plausible and give reasonable results, we note that they are purely phenomenological.
[28]To put the two curves of Fig. 4(b) in one plot for the comparison, we have shifted the potential energy for the case without exchange energy by a constant factor of $-1.122(2R_y)$.
[29]Once again, for the purpose of plotting clearly, we have shifted the potential values in Fig. 5, for $z = a_B$ and $z = 0$, by adding constants 4.19 and 6.27, respectively.
[30]C. S. Lent, J. Appl. Phys. **67**, 6353 (1990).
[31]Yongjiang Wang, Jian Wang, and Hong Guo, Phys. Rev. B **49**, 1928 (1994).
[32]A. Szafer and B. Altshuler, Phys. Rev. Lett. **70**, 587 (1993).
[33]M. Gutzwiller, *Chaos in Classical and Quantum Mechanics* (Springer Verlag, New York, 1991).
[34]J. Wang, Y. Wang, and H. Guo, Appl. Phys. Lett. **65**, 1793 (1994).
[35]All the numerical calculations presented here were performed on a Silicon-Graphics workstation.